Internal fluctuations, period doubling, and chemical chaos

Xiao-Guang Wu and Raymond Kapral
Chemical Physics Theory Group, Department of Chemistry, University of Toronto, Toronto, Ontario, Canada M5S 1A1
(Received 18 May 1994)

The effects of internal molecular fluctuations on period-doubling bifurcations and chaotic band merging are studied in a well-stirred reactive chemical system where spatial degrees of freedom play no role. The calculations are carried out using a stochastic model based on reactive lattice-gas cellular automata. Molecular fluctuations arising from reactive collisions are incorporated in the model and the mass-action rate equations are recovered in the mean field limit. Large system sizes can be studied and permit the investigation of the internal noise scaling structure in the periodic and chaotic regimes. For the Willamowski-Rössler system the noise scaling exponent is consistent with that found for one-dimensional quadratic maps subject to external noise. The model provides a means to study small, nonequilibrium, reacting systems where fluctuations may not be neglected.

PACS number(s): 05.45.+b, 05.40.+j

I. INTRODUCTION

The effects of external noise on period-doubling bifurcations and band merging within the chaotic regime were studied [1,2] shortly after the renormalization treatment of the scaling structure of this bifurcation scenario was reported [3]. The most detailed investigations considered the discrete-time noisy dynamical system

$$x(t+1) = f(x(t)) + \xi(t) , \tag{1}$$

where $f(x)$ is some nonlinear function, usually with a single quadratic extremum, and ξ is a noise term, often taken to be Gaussian white noise with amplitude σ. It is clear that external noise can disrupt the period-doubling cascade. Noise will obliterate some of the periodic structure in the period-doubling sequence and shift the bifurcation points. Similarly, within the chaotic region, noise can lead to merging of the chaotic bands and destroy some of the fine structure of the chaotic attractor. Both of these features were observed to satisfy a scaling structure [1,2,4]. For example, if σ_n is the noise amplitude for which an orbit of at most period 2^n can be observed, then $\lim_{n\to\infty} \sigma_n/\sigma_{n+1} = \beta$, where $\beta \approx 6.6$ [1,2,4] for maps with a quadratic extremum. A similar scaling applies for the band merging process in the chaotic regime. External noise effects have also been explored near intermittency transitions to chaos [5], for transitions to chaos via quasiperiodicity [6], and for a variety of other types of external noise sources [7].

The effects of internal molecular fluctuations on nonlinear dynamical systems have also been studied [8–12]. For systems subject to external noise the form of the noise term can be specified independently of the system dynamics, although it may be chosen to depend on the dynamical variable. In contrast, internal noise arises directly from the microscopic dynamics and its study involves more delicate issues since the magnitude of the noise is in part determined by the microscopic or mesoscopic description of the system. Consider, for example, a chemically reacting system displaced far from equilibrium by external flows of reagents. The fluctuations experienced by the system arise from the random reactive collision events and motions of the molecules making up the reacting mixture. Thus the noise fluctuations are determined by the chemical mechanism, diffusion, and system size. Approximate Fokker-Planck or Langevin descriptions [8,9], master equation models [10], and reactive lattice-gas automaton models [11,12] have been employed to investigate various aspects of this problem.

In this paper we examine the effects of internal molecular fluctuations on period-doubling bifurcations and chaos in a chemically reacting system. We restrict our attention to well-stirred reacting mixtures where the only source of fluctuations is the chemical species number changes that arise from the random reactive events. Our calculations are carried out for the Willamowski-Rössler (WR) reaction [13], whose mechanism reads

$$\begin{aligned} &A_1 + X \underset{k_{-1}}{\overset{k_1}{\rightleftharpoons}} 2X, \quad X + Y \underset{k_{-2}}{\overset{k_2}{\rightleftharpoons}} 2Y, \\ &A_5 + Y \underset{k_{-3}}{\overset{k_3}{\rightleftharpoons}} A_2, \quad X + Z \underset{k_{-4}}{\overset{k_4}{\rightleftharpoons}} A_3, \\ &A_4 + Z \underset{k_{-5}}{\overset{k_5}{\rightleftharpoons}} 2Z . \end{aligned} \tag{2}$$

This mechanism, which is based on a realistic mass-action reaction scheme, focuses on the dynamics of the intermediate chemical species, X, Y, and Z. The concentrations of the remaining species A_i, $i = 1,\ldots,5$, are assumed to be held fixed by external flows of reagents. The concentrations of these constrained chemical species, along with the values of the rate constants $k_{\pm i}$, $i = 1,\ldots,5$, constitute the bifurcation parameters for the problem.

The phenomenological rate law corresponding to this mechanism is

$$\frac{d\bar{\rho}_x}{dt} = R_x(\bar{\boldsymbol{\rho}}) = \kappa_1\bar{\rho}_x - \kappa_{-1}\bar{\rho}_x^2 - \kappa_2\bar{\rho}_x\bar{\rho}_y + \kappa_{-2}\bar{\rho}_y^2 - \kappa_4\bar{\rho}_x\bar{\rho}_z + \kappa_{-4} ,$$

$$\frac{d\bar{\rho}_y}{dt} = R_y(\bar{\boldsymbol{\rho}}) = \kappa_2\bar{\rho}_x\bar{\rho}_y - \kappa_{-2}\bar{\rho}_y^2 - \kappa_3\bar{\rho}_y + \kappa_{-3} , \quad (3)$$

$$\frac{d\bar{\rho}_z}{dt} = R_z(\bar{\boldsymbol{\rho}}) = -\kappa_4\bar{\rho}_x\bar{\rho}_z + \kappa_{-4} + \kappa_5\bar{\rho}_z - \kappa_{-5}\bar{\rho}_z^2 .$$

Here the constant concentrations of species A_i have been incorporated into the set of rate coefficients $\kappa_{\pm i}$, $i = 1,\ldots,5$, and $\bar{\boldsymbol{\rho}} = (\bar{\rho}_x, \bar{\rho}_y, \bar{\rho}_z)$ with $\bar{\rho}_\tau$ ($\tau = x, y, z$ or $\tau = 1, 2, 3$; we use this notation interchangeably) the average concentration of species τ. Chaos is possible in such a three-dimensional, dissipative, nonlinear dynamical system and, indeed, a strange attractor is observed to arise as result of a period-doubling cascade for suitable choices of the κ_i parameters (cf. the bifurcation diagram in Fig. 1 of Ref. [12] and Refs. [13] and [14]). Thus, this model can be used to investigate internal fluctuation effects on the period-doubling cascade and chaos once a microscopic or mesoscopic description of the reaction dynamics is given [11,12].

In Sec. II we present a mesoscopic model of the reaction dynamics that incorporates molecular fluctuations and leads, in the mean field limit, to the deterministic rate law (3). In this section we also describe the scheme used to simulate the reactive dynamics and present qualitative results on the structure of the noisy attractors and the invariant density in both the periodic and chaotic regimes as a function of the system size. In Sec. III we discuss the computation of the noisy Lyapunov exponents used to characterize the dynamical state of the system and give a quantitative discussion of internal noise effects on the period-doubling cascade in this reactive system. Finally, the conclusions of our study are given in Sec. IV.

II. STOCHASTIC WILLAMOWSKI-RÖSSLER DYNAMICS

The stochastic model we employ to study fluctuation effects on the period-doubling cascade is derived from the well-stirred limit of the reactive lattice-gas cellular automaton description of the dynamics [11,12]. In the automaton, reactive species are assigned positions and discrete velocities on a lattice and their evolution is governed by the composition of propagation, velocity randomization, and chemical transformation operators [15–17]. Each chemical species τ resides on its own species lattice $\mathcal{L}_\tau$ and is subject to an exclusion principle such that no more than one particle of a given species with a given velocity may reside at a node of the lattice. This implies that the particle occupancies α_τ for species τ at a node lie in the range $0 \le \alpha_\tau \le m$, where m is the coordination number of the lattice. In our calculations we use hexagonal lattices with $m = 6$.

The treatment of reactive particle number fluctuations in the automaton is similar in spirit to that in birth-death master equation methods [18]. The reaction probability matrix that specifies how reactions occur in the model is based on the underlying chemical mechanism and is therefore expected to provide a realistic description of the species number fluctuations. The validity of of such a model has been tested in detail for the Schlögl reaction where space-time concentration correlations have been shown to be in accord with standard stochastic models in the hydrodynamic regime [19].

In the well-stirred limit, the distribution of particles at the nodes of the lattice is always binomial. Spatial pattern formation is not possible since mixing destroys any spatial structure and fluctuations arise from the random reactive events in the system. Consequently, our focus is on how the bulk reactive particle number fluctuations influence the dynamics of the global concentrations of the chemical species. Some aspects of the well-stirred dynamics in the Willamowski-Rössler system were considered earlier [11,12]; here we shall give a quantitative description of noise effects on the period-doubling bifurcations and chaos.

A. Markov chain

In the well-stirred limit the dynamics can be described by a Markov chain for particle number changes [12]:

$$P(\mathbf{n}, t+1) - P(\mathbf{n}, t) = \sum_{\mathbf{n}'} [P(\mathbf{n}', t)W(\mathbf{n}'|\mathbf{n}) - P(\mathbf{n}, t)W(\mathbf{n}|\mathbf{n}')] , \quad (4)$$

or

$$P(\mathbf{n}, t+1) = \sum_{\mathbf{n}'} P(\mathbf{n}', t)W(\mathbf{n}'|\mathbf{n}) . \quad (5)$$

Here $P(\mathbf{n}, t) = P(n_1, n_2, n_2, t)$ is the joint probability of finding n_1 particles of species $X_1 = X$ on lattice $\mathcal{L}_1$, n_2 particles of species $X_2 = Y$ on lattice $\mathcal{L}_2$, and n_3 particles of species $X_3 = Z$ on lattice $\mathcal{L}_3$ at time t. The probability of transition from an initial particle number configuration $\mathbf{n}$ to a final particle number configuration $\mathbf{n}'$ is $W(\mathbf{n}|\mathbf{n}')$ and can be expressed as [12]

$$W(\mathbf{n}|\mathbf{n}') = \prod_{\tau=1}^{3} \left[\sum_{\substack{n_{\tau+}, n_{\tau-} \\ n_{\tau+} - n_{\tau-} = n'_\tau - n_\tau}} P_\tau(n_{\tau+}, n_{\tau-}|\boldsymbol{\rho}(t)) \right] , \quad (6)$$

where $P_\tau(n_{\tau+}, n_{\tau-}|\boldsymbol{\rho})$ is the probability of $n_{\tau+}$ particle number transformations $\alpha_\tau \to \alpha_\tau + 1$ and $n_{\tau-}$ particle number transformations $\alpha_\tau \to \alpha_\tau - 1$ on lattice $\mathcal{L}_\tau$ which has $\mathcal{N}$ nodes (and thus $n'_\tau - n_\tau = n_{\tau+} - n_{\tau-}$), with the condition that the densities on the three species lattices are $\boldsymbol{\rho} = \mathbf{n}/\mathcal{N}$. Note that the WR mechanism involves particle number changes by ± 1 particle in each reaction step; hence the restriction to such changes in the elements making up the transition probability matrix. The probability $P_\tau(n_{\tau+}, n_{\tau-}|\boldsymbol{\rho})$ is

$$P_\tau(n_{\tau+},n_{\tau-}|\boldsymbol{\rho}) = \frac{\mathcal{N}!}{n_{\tau+}!n_{\tau-}!(\mathcal{N}-n_{\tau+}-n_{\tau-})!} \times (P_\tau^+)^{n_{\tau+}}(P_\tau^-)^{n_{\tau-}} \times (1-P_\tau^+-P_\tau^-)^{\mathcal{N}-n_{\tau+}-n_{\tau-}}, \quad (7)$$

where $P_\tau^+ = P_\tau^+(\boldsymbol{\rho})$ and $P_\tau^- = P_\tau^-(\boldsymbol{\rho})$ are transition probabilities averaged over the binomial distribution on lattice $\mathcal{L}_\tau$. The explicit forms follow from the definition of the reaction probability matrix and are given in the Appendix.

From these expressions we can derive the discrete-time form of the mass-action rate law (3). Since the average densitiy of species τ is defined as

$$\bar{\rho}_\tau(t) = \frac{1}{\mathcal{N}}\sum_{\mathbf{n}} n_\tau P(\mathbf{n},t), \quad (8)$$

it follows from (4) that

$$\begin{aligned}\bar{\rho}_\tau(t+1)-\bar{\rho}_\tau(t) &= \frac{1}{\mathcal{N}}\sum_{\mathbf{n}} n_\tau \left\{ \sum_{\mathbf{n}'\neq\mathbf{n}} W(\mathbf{n}'|\mathbf{n})P(\mathbf{n}',t) - \left[\sum_{\mathbf{n}'\neq\mathbf{n}} W(\mathbf{n}|\mathbf{n}')\right] P(\mathbf{n},t)\right\} \\ &= \frac{1}{\mathcal{N}}\sum_{\mathbf{n}}\sum_{n_{\tau+},n_{\tau-}} (n_{\tau+}-n_{\tau-})P_\tau(n_{\tau+},n_{\tau-}|\boldsymbol{\rho})P(\mathbf{n},t) \\ &= \sum_{\mathbf{n}} hR_\tau(\mathbf{n}/\mathcal{N})P(\mathbf{n},t) = h\overline{R_\tau(\boldsymbol{\rho}(t))}, \end{aligned} \quad (9)$$

where an overbar indicates an average over $P(\mathbf{n},t)$ as in (8). Averages over the probability distribution $P_\tau(n_{\tau+},n_{\tau-}|\boldsymbol{\rho}(t))$ depend on $\boldsymbol{\rho}(t)$ and will be denoted by $\langle\cdots\rangle$. Thus, $R_\tau(\boldsymbol{\rho}(t))$ may also be written as

$$\begin{aligned} hR_\tau(\boldsymbol{\rho}(t)) &= \langle n_{\tau+}\rangle - \langle n_{\tau-}\rangle \\ &= \mathcal{N}P_\tau^+ - \mathcal{N}P_\tau^- . \end{aligned} \quad (10)$$

Note that the argument of R_τ is a random vector. The mass-action rate law is recovered when $\overline{R_\tau(\boldsymbol{\rho}(t))}$ is replaced by $R_\tau(\bar{\boldsymbol{\rho}}(t))$ [cf. (3)]. In this limit we have

$$\bar{\rho}_\tau(t+1)-\bar{\rho}_\tau(t) = hR_\tau(\bar{\boldsymbol{\rho}}(t)) . \quad (11)$$

The parameter h sets the time scale used in the construction of the reaction probability matrix and as h tends to zero the continuous-time mass-action rate law (3) is recovered.

We choose $P_\tau^\pm \ll 1$ so that reaction is a rare event. This limit can be achieved by a suitable choice of the time scale h. In this case the transition probability $P_\tau(n_{\tau+},n_{\tau-}|\boldsymbol{\rho})$ is sharply peaked around $(\langle n_{\tau+}\rangle,\langle n_{\tau-}\rangle)$. Then, for given $n_{\tau\pm}$, in the limit $\mathcal{N}\to\infty$, $P_\tau^\pm \to 0$ with $\mathcal{N}P_\tau^\pm$ constant, the trinomial distribution (7) reduces to a product of two Poisson distributions, i.e.,

$$P_\tau(n_{\tau+},n_{\tau-}|\boldsymbol{\rho}) = \mathcal{P}_\tau(n_{\tau+}|\boldsymbol{\rho})\mathcal{P}_\tau(n_{\tau-}|\boldsymbol{\rho}), \quad (12)$$

where

$$\mathcal{P}_\tau(n_{\tau\pm}|\boldsymbol{\rho}) = \frac{(\mathcal{N}P_\tau^\pm)^{n_{\tau\pm}}}{n_{\tau\pm}!}\exp(-\mathcal{N}P_\tau^\pm). \quad (13)$$

If $\mathcal{N}$ is large enough so that $\langle n_{\tau\pm}\rangle = \mathcal{N}P_\tau^\pm \gg 1$ for all τ and t then the trinomial distribution (7) reduces to a product of two Gaussian distributions of the form

$$\mathcal{P}_\tau(n_{\tau\pm}|\boldsymbol{\rho}) = \frac{1}{(2\pi)^{1/2}\mathcal{N}\sigma_\tau^\pm}\exp\left[-\frac{(n_{\tau\pm}/\mathcal{N}-P_\tau^\pm)^2}{2(\sigma_\tau^\pm)^2}\right], \quad (14)$$

with $\sigma_\tau^\pm = (P_\tau^\pm/\mathcal{N})^{1/2} = \epsilon(P_\tau^\pm)^{1/2}$, where $\epsilon = \mathcal{N}^{-1/2}$.

B. Stochastic simulations

The particle number changes that occur as a result of the random reactive events are given by the stochastic equation

$$\mathbf{n}(t+1) = \mathbf{n}(t) + \mathbf{n}_+(\mathbf{n}(t)) - \mathbf{n}_-(\mathbf{n}(t)), \quad (15)$$

where the random variables $\mathbf{n}_\pm$ have Poisson distributions (13) under the conditions discussed above. This equation provides the basis for a stochastic simulation of the reactive dynamics that allows very large system sizes to be studied, a requirement for the investigation of internal noise effects on the period-doubling cascade. The dynamics determined by (15) can be simulated by selecting $\mathbf{n}_\pm$ at each time step from the Poisson distributions (13), which are functions of the instantaneous density $\boldsymbol{\rho}(t)$.

In the simulation results presented below we take κ_2 as the bifurcation parameter. All the other rate coefficients are held constant: $\kappa_1 = 31.2$, $\kappa_{-1} = 0.2$, $\kappa_{-2} = 0.1$, $\kappa_3 = 10.8$, $\kappa_{-3} = 0.12$, $\kappa_4 = 1.02$, $\kappa_{-4} = 0.01$, $\kappa_5 = 16.5$, and $\kappa_{-5} = 0.5$. The results of simulations of the stochastic equation (15) for the WR system in the chaotic regime are shown in Fig. 1 for two different system sizes, $\mathcal{N} = (1024)^2$ and $\mathcal{N} = (4096)^2$. For comparison, the deterministic chaotic attractor is shown in the bottom panel and has a banded structure [20]. As expected, for the stochastic dynamics the structure of these bands can be resolved with greater precision as the system size increases. Note also that quite large system sizes are required to resolve even the first and second bands. In the middle panel for $\mathcal{N} = (4096)^2$ sites per lattice the four-band structure is just visible. We shall investigate these effects quantitatively in the next section.

The invariant distribution $P(\mathbf{n}) = \lim_{t\to\infty} P(\mathbf{n},t)$ may be obtained from a time average of the Kronecker δ

$$P_\epsilon(\mathbf{n}) = \lim_{T\to\infty} T^{-1}\sum_{t=0}^{T}\delta_{n_\tau - n_\tau(t)} . \quad (16)$$

Here n_τ is a prescribed value of $n_\tau(t)$, and the subscript ϵ is appended to specify the noise amplitude ($\epsilon = \mathcal{N}^{-1/2}$). A convenient way to represent the invariant distribution is to consider its structure in a Poincaré section of the phase-space flow. The Poincaré section $\mathcal{P}$ chosen for this purpose is shown in Fig. 1, top panel, and is defined by

$$\{\mathcal{P} : \rho_x/x_M = 0.316\,667, \forall \rho_y/y_M \geq 0, \forall \rho_z/z_M \geq 0\}, \tag{17}$$

where τ_M, $\tau = x$, y, and z are scale factors [12]. Any phase-space trajectory $\boldsymbol{\rho}(t) = (\rho_x(t), \rho_y(t), \rho_z(t))$ that crosses the section from the high X concentration side will produce a point $\mathbf{x} = (y, z)$ in this section. Figure 2 shows the Poincaré maps for both the stochastic model [$\mathcal{N} = (500)^2$] and the deterministic system for $\kappa_2 = 1.572$ in the chaotic regime. For this very small system size internal noise completely destroys the phase coherence that is responsible for the banded structure of the deterministic chaotic attractor; however, the noisy iterates are still confined to a linelike segment indicating that internal noise has a dominant effect along the unstable directions of the phase-space flow [11,12].

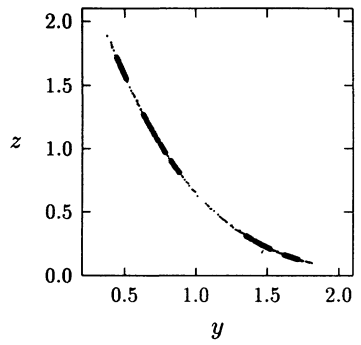

FIG. 2. Poincaré maps of the stochatic WR model [small dots, $\mathcal{N} = (500)^2$] and the deterministic dynamics (heavy dots) for $\kappa_2 = 1.572$.

Since the points $\mathbf{x}(t)$ on $\mathcal{P}$ are distributed in a linelike fashion (cf. Fig. 2) one may model the stochastic dynamics as an endomorphism of the line. We construct the endomorphism from the Poincaré map by letting s denote the distance along the Poincaré map with the origin of s taken to lie at one end. Each $\mathbf{x}(t)$ then corresponds to an s value $s(t)$ and the one-dimensional map has the form $s(t+1) = f_R(s(t))$, where $f_R(s(t))$ is a random nonlinear map whose form can in principle be obtained from the full stochastic dynamics but is difficult to construct. Figure 3 shows the one-dimensional map for the parameter $\kappa_2 = 1.537$ corresponding to period 4 for a system size with $\epsilon = 4 \times 10^{-4}$ (small points). The deterministic period-4 fixed points are shown as open circles. The noisy dynamics comprises two bands that encompass the two pairs of fixed points. For comparison, the solid line is a fit of the stochastic dynamics to a quadratic function ($s_{t+1} = 1.387\,126 + 1.746\,474\, s_t - 1.061\,821\, s_t^2$). Figure 4 shows a plot of the invariant distribution $P_\epsilon(s)$ for $\kappa_2 = 1.537$ for two different noise amplitudes. For $\epsilon = 4 \times 10^{-4}$ [$\mathcal{N} = (2500)^2$] $P_\epsilon(s)$ possesses four sharp maxima, corresponding to the four bands of the noisy at-

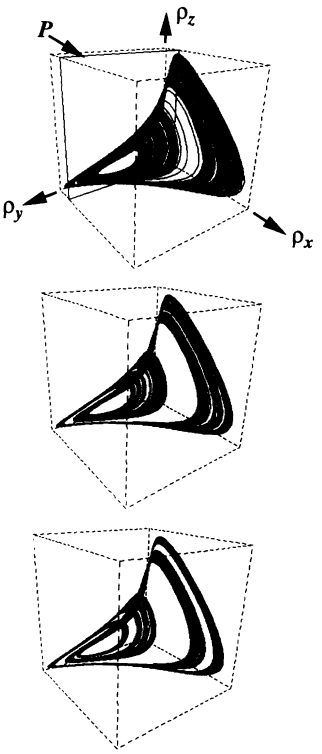

FIG. 1. Three-dimensional plot of phase-space trajectories obtained using the stochastic simulation method for $\mathcal{N} = (1024)^2$ (top) and $\mathcal{N} = (4096)^2$ (middle). The deterministic attractor is shown in the bottom panel. The bifurcation parameter was chosen so that the system is in the chaotic regime, i.e., $\kappa_2 = 1.571$, and the trajectories were obtained by following the motion of phase point $\rho_\tau(t) = n_\tau(t)/\mathcal{N}$ in the three-dimentional concentration phase space. The dashed box containing the attractor has its origin at (0.070 64, 0.002 76, 0.111 90) and corners along the ρ_x, ρ_y, and ρ_z axes at 1.801 29, 1.759 82, and 4.287 91, respectively. The Poincaré section, defined in (17), is shown in the top panel and labeled by $\mathcal{P}$.

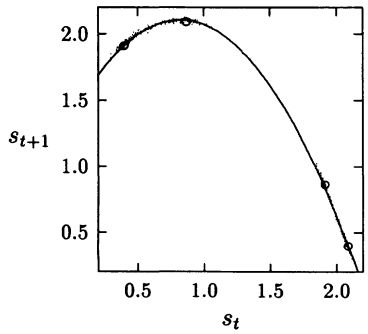

FIG. 3. Next amplitude map constructed from the Poincaré map for a superstable period-4 orbit ($\kappa_2 = 1.537$) with $\epsilon = 4 \times 10^{-4}$. The open circles are for deterministic dynamics and the solid line is the best quadratic fit.

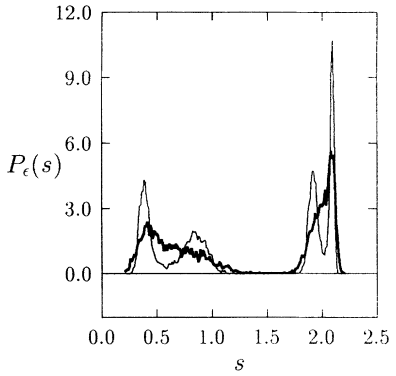

FIG. 4. Invariant distribution $P_\epsilon(s)$ for $\kappa_2 = 1.537$ and different system sizes $\mathcal{N} = (1250)^2$ (thick line) (the Lyapunov exponent is $\lambda \approx -2.03 \times 10^{-2}$) and $\mathcal{N} = (2500)^2$ (the Lyapunov exponent is now positive, $\lambda \approx 0.91 \times 10^{-2}$)(thin line).

tractor which are centered around the four period-4 fixed points of the deterministic system. Note that the two pairs of maxima are separated by a region of very small probability density (zero in our finite-time simulations) but the two maxima comprising a pair are separated by a region of small but nonzero probability densities. Thus, although from Fig. 3 it may appear that period 4 cannot be resolved for this system size, the stationary probability density and, as we shall see below, the Lyapunov exponent, indicate that a noisy period-4 orbit can be identified. For $\epsilon = 8 \times 10^{-4}$ [$\mathcal{N} = (1250)^2$] $P_\epsilon(s)$ shows only two peaks and the period-4 structure is no longer seen.

When the system parameters are chosen in the chaotic regime the system is very sensitive to perturbations and even very weak noise may destroy some of the fine structure of $P(s)$, the deterministic invariant distribution (cf. Fig. 5). As the noise level increases all of the detailed structure of $P(s)$ is destroyed but the width of the distribution changes little (cf. Fig. 5; see also Refs. [9–12]). As can be seen in this figure, the deterministic invariant distribution has extensive fine structure, only some of which is resolved for a small value of $\epsilon = 10^{-5}$ ($\mathcal{N} = 10^{10}$).

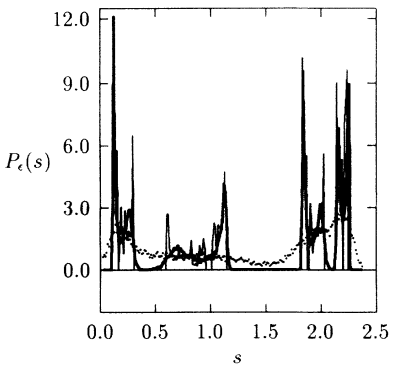

FIG. 5. Invariant distribution $P_\epsilon(s)$ for $\kappa_2 = 1.572$ and different noise amplitudes $\epsilon = 10^{-5}$ (thick line) and $\epsilon = 2 \times 10^{-4}$ (dotted line). The deterministic result $[P(s)]$ for the same system parameters is shown as a thin line.

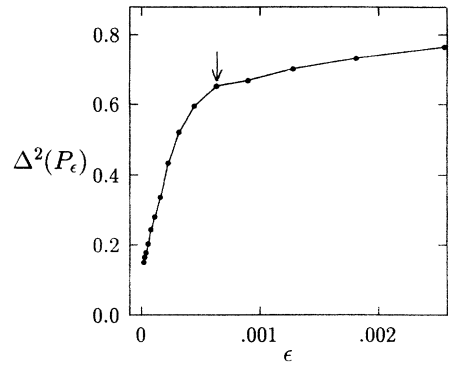

FIG. 6. Deviation $\Delta^2(P_\epsilon)$ as function of the noise amplitude ϵ for $\kappa_2 = 1.572$. The arrow indicates the ϵ value where the gap in the two-band attractor just vanishes.

We define the deviation of the invariant distribution of the stochastic WR model, $P_\epsilon(s)$, from that of deterministic dynamics, $P(s)$, as

$$\Delta^2(P_\epsilon) = \left[\int ds P(s)^2\right]^{-1} \int ds [P_\epsilon(s) - P(s)]^2 . \quad (18)$$

Figure 6 plots the deviation $\Delta^2(P_\epsilon)$ versus ϵ for a chaotic attractor ($\kappa_2 = 1.572$). For the ϵ range explored in this figure the chaotic attractor contains the two bands for small ϵ or no bands for large ϵ. The rapid increase in Δ^2 occurs as the internal noise causes the probability mass to fill the gap along s in the two-band chaotic attractor. For sufficiently small system sizes the gap has filled and Δ^2 increases much more slowly with decreases in system size since only small overall expansions and smoothing of the attractor occur.

III. SCALING IN THE PERIOD-DOUBLING REGIME

We next quantitatively characterize the effects of internal noise on the periodic orbits lying within the period-doubling cascade. In Fig. 7 we show a noise bifurca-

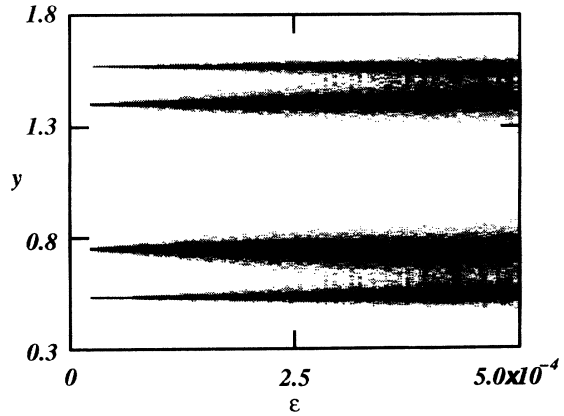

FIG. 7. Noise bifurcation diagram for $\kappa_2 = 1.537$ (superstable period-4 orbit). The ordinate y is the ρ_y value on $\mathcal{P}$.

tion diagram at a fixed parameter $\kappa_2 = 1.537$ (period-4 regime) with ϵ varing from 2×10^{-5} to 5×10^{-4}. Internal fluctuations alter the structure of the period-4 orbit and the ability to resolve such an orbit in the period-doubling cascade depends on the degree to which the noise is able to dephase the periodic dynamics. Such dephasing can be discussed in terms of phase basins and their boundaries [21]. A period-n orbit will intersect a Poincaré plane in n fixed points which are visited in a definite order. A phase basin consists of all initial points that tend to a given fixed point in a stroboscopic representation of the dynamics. The phase plane can be partitioned into n phase basins separated by phase basin boundaries which can be complicated or even fractal. Noise-induced crossing of a phase basin boundary leads to a loss of phase coherence and is ultimately responsible for the inability to resolve a given period orbit.

In order to determine the ϵ value at which a given periodic orbit can no longer be resolved we consider a set of equivalent parameter values corresponding to the superstable points of the period-2^n orbits and make use of the Lyapunov exponent to detect when the character of the noisy dynamics changes [22]. In the presence of fluctuations the Lyapunov exponent can be determined by considering the linearized dynamics along a noisy orbit [7,23,24]. In this way the Lyapunov exponent measures the separation of nearby orbits which experience fluctuations derived from the same underlying stochastic process. This procedure has the advantage that noise effects arising from different realizations of the stochastic process do not contribute to the Lyapunov exponent. More specifically, for a noisy system the maximum Lyapunov exponent can be computed from the following expression [7]:

$$\lambda = \lim_{N_R \to \infty} (N_R T)^{-1} \sum_{j=1}^{N_R} \ln[d^{(j)}(T)/d^{(j)}(0)] . \tag{19}$$

Here $d(t) = |\mathbf{d}(t)| = |\boldsymbol{\rho}(t) - \boldsymbol{\rho}'(t)|$ is the magnitude of the separation between two neighboring phase-space trajectories calculated with the same random number string, and the superscript j indicates one of the N_R different realizations of the stochastic dynamics. Since the Lyapunov exponent is a measure of the average exponential growth rate of neighboring phase-space trajectories the time T in (19) should be chosen such that $d(t) < d_{\max}$, $\forall t \leq T$. Here $d_{\max}$ is a value of d below which the linearized dynamics for relative separation is valid.

The stochastic dynamics of the WR model is given by (15) which may be written in the form

$$\begin{aligned} \rho_\tau(t+1) &= \rho_\tau(t) + hR_\tau(\boldsymbol{\rho}(t)) + \xi_\tau(t) \\ &\equiv \mathcal{R}_\tau(\boldsymbol{\rho}(t)) + \xi_\tau(t) , \end{aligned} \tag{20}$$

where $\xi_\tau(t)$ is a random force with zero mean defined by

$$\xi_\tau(t) = \mathcal{N}^{-1}\{\delta n_{\tau+}(\boldsymbol{\rho}(t)) - \delta n_{\tau-}(\boldsymbol{\rho}(t))\}, \tag{21}$$

with $\delta n_{\tau\pm} = n_{\tau\pm} - \langle n_{\tau\pm} \rangle$. In order to compute $d_\tau(t)$ using this equation we adopt the method described above. We select $\boldsymbol{\rho}'(0) = \boldsymbol{\rho}(0) + \delta\boldsymbol{\rho}$ and let $\boldsymbol{\rho}'(t)$ be the value of the density at time t starting from $\boldsymbol{\rho}'(0)$ and using equation (20) with the same random number string used to produce $\boldsymbol{\rho}(t)$ starting from $\boldsymbol{\rho}(0)$. Using the definition of $\mathbf{d}$ and (20) we find

$$\begin{aligned} d_\tau(t+1) &= d_\tau(t) + h\,[R_\tau(\boldsymbol{\rho}'(t)) - R_\tau(\boldsymbol{\rho}(t))] + \Delta\xi_\tau(t) \\ &\approx \sum_{\tau'} \{\delta_{\tau\tau'} + hJ_{\tau\tau'}(\boldsymbol{\rho}(t))\}\, d_{\tau'}(t) + O(\mathcal{N}^{-1/2}) . \end{aligned} \tag{22}$$

Here $J_{\tau\tau'}$ $(\tau, \tau' = 1, 2, 3)$ are elements of the Jacobian matrix and $\Delta\xi_\tau = \xi_\tau(\boldsymbol{\rho}'(t)) - \xi_\tau(\boldsymbol{\rho}(t))$, which is $O(\mathcal{N}^{-1/2})$. Thus the distance between trajectories may be computed from the linearized dynamics along the stochastic trajectory generated by (20).

Using the algorithm of Benettin *et al.* [25], the maximum Lyapunov exponent may be computed from the expression

$$\lambda = \lim_{t \to \infty} t^{-1} \ln\{d(t)/d(0)\} . \tag{23}$$

Here the λ can be regarded as the average slope of the function $\Lambda(t) = \ln\{d(t)/d(0)\}$ [26]. Plots of $\Lambda(t)$ versus t are shown in Fig. 8 for the noisy dynamics in the chaotic regime ($\kappa_2 = 1.572$) and in the period-4 regime ($\kappa_2 = 1.537$) for two values of ϵ. Note how the noise amplitude influences the slope of $\Lambda(t)$ in the periodic regime.

The maximum Lyapunov exponent is plotted versus ϵ in Fig. 9(a). One can see that the Lyapunov exponent is negative for sufficiently small ϵ and increases to positive values as ϵ increases [26]. The Lyapunov exponent λ passes through zero at $\epsilon \approx 6.8 \times 10^{-4}$ [Fig. 9(a)]. The Lyapunov exponent for a chaotic orbit at different noise levels is shown in Fig. 9(b). We see that λ increases rapidly when ϵ is small; it then reaches a plateau value where noise affects it very little. The rapid increase of λ corresponds to a noise regime where merging between adjacent chaotic bands takes place. The noise regime explored in this figure corresponds roughly to that in the top two panels of Fig. 1; thus the period-4 chaotic band structure has been destroyed by decreasing the system

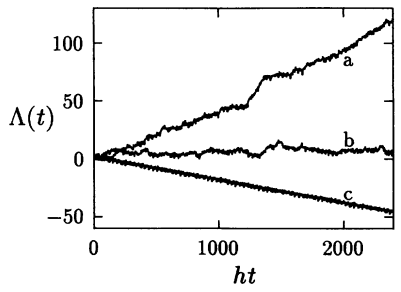

FIG. 8. Plot of $\Lambda(t) = \ln\{d(t)/d(0)\}$ with $h = 1.5 \times 10^{-4}$ for (a) $\kappa_2 = 1.572$ and $\epsilon = 6 \times 10^{-4}$, (b) $\kappa_2 = 1.537$ and $\epsilon = 6.4 \times 10^{-4}$, and (c) $\kappa_2 = 1.537$ and $\epsilon = 2 \times 10^{-4}$. The three corresponding Lyapunov exponents are average slopes of the three curves and are given by $\lambda = 5.01 \times 10^{-2}$, 0, and -1.88×10^{-2}, respectively.

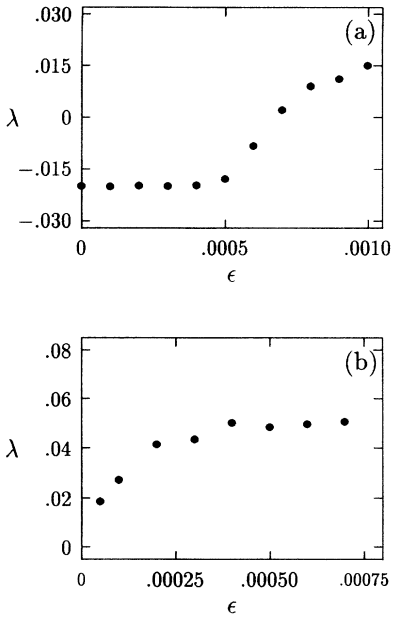

FIG. 9. Lyapunov exponent as a function of the noise level ϵ for (a) the superstable period-4 orbit at fixed parameter $\kappa_2 = 1.537$ and (b) a chaotic orbit at $\kappa_2 = 1.572$.

size. When band merging is complete, increasing noise level has a less pronounced effect on the distribution of phase points so the Lyapunov exponent changes very little. The process is analogous to that discussed earlier in connection with Fig. 6 (see also Ref. [9]).

Internal noise also alters the bifurcation diagram. The position of a period-doubling bifurcation in parameter space can be determined from the behavior of the Lyapunov exponent(s) as a function of the bifurcation parameter. In the presence of internal noise we have found that the period-1 bifurcation point is shifted to slightly higher values of κ_2.

We may now bring these observations to bear on the internal noise scaling in the period-doubling regime. As noted above we observe the noisy dynamics at equivalent parameter values (superstable points) within the period-2^n regimes. For each such parameter value the noise amplitude is varied until the maximum Lyapunov exponent passes through zero. The corresponding value of ϵ for a period-2^n orbit will be denoted by ϵ_n^+. Calculations were carried out for orbits with periods up to eight and the results are $\epsilon_2^+/\epsilon_4^+ = 4.2 \times 10^{-3}/6.3 \times 10^{-4} \approx 6.7$, and $\epsilon_4^+/\epsilon_8^+ = 6.3 \times 10^{-4}/1.04 \times 10^{-4} \approx 6.1$.

Given the small uncertainties in the locations of the superstable points and in the estimation of the noisy Lyapunov exponents, these results are consistent with the scaling exponent $\beta \approx 6.6$ obtained earlier for external noise on one-dimensional maps. The calculations are rather difficult to carry out for higher members of the period-doubling cascade since very large system sizes must be studied in order to resolve the higher-period orbits. Even to resolve period-8 system sizes of the order of $\mathcal{N} \approx 10^8$ particles must be considered. In view of the fact that the kernel in the Perron-Frobenius equation corresponding to the three-dimensional dynamics (20) is Gaussian and the noisy map in the Poincaré plane is quadratic in s with probability density sharply peaked normal to s, such a scaling relation for internal noise is plausible.

IV. CONCLUSION

The effects of chemical species number fluctuations on the nonlinear WR reaction dynamics in both the period-doubling and chaotic regimes were explored for large systems using a stochastic model based on the reactive lattice-gas automaton method. In the period-doubling regime the simulations showed that internal noise scaling follows the same scaling laws as external noise, namely, if the noise amplitude is such that a period-2^n orbit may be resolved, in order to resolve an orbit with period 2^{n+1} the noise amplitude must be reduced by a factor of approximately 6.6. For the internal noise process considered here the noise amplitude is controlled by varying the system size. Our stochastic calculations were able to resolve orbits up to period 8 for systems with approximately 10^8 particles. This implies that in macroscopic well-stirred systems containing roughly a mole of molecules at least five or six more period doublings could be resolved if the systems were perfectly homogeneous and external noise played no role. Therefore, most likely the inability of chemical experiments to resolve higher-order members of the period-doubling cascade (usually only orbits up to period 8 have been resolved in experiments) is due to inhomogeneities in the reactor and other sources of external experimental noise.

The simulations show that even for fairly small systems on the macroscopic scale (comprised of roughly 10^{10} particles) one may resolve the higher members of a banded chaotic attractor, confirming that internal noise, like external noise, destroys the fine structure of of the chaotic attractor but its gross features are robust to such internal fluctuations. While the scaling structure of chaotic band merging was not investigated in detail here, the results suggest that scaling similar to that observed for one-dimensional maps applies.

The calculations indicate that for macroscopic chemical systems internal noise effects arising from local inhomogeneities or imperfect mixing, or effects due to external noise sources, are more likely sources of perturbation of the dynamics in the period-doubling regime than those due to bulk species number fluctuations arising from reaction. For smaller system sizes in the mesoscopic regime internal fluctuations, even in the well-stirred limit, can have important effects. What is perhaps most interesting is that the gross structure of chaotic attractors survives even for very small system sizes. Since new chemistry can occur in small systems and experimental probes of reaction dynamics and even pattern formation are now possible on small scales, stochastic models of the sort considered here provide a means to study the effects of fluctuations on small, far-from-equilibrium, reacting systems.

ACKNOWLEDGMENTS

This work was supported in part by a grant from the Natural Sciences and Engineering Research Council of Canada.

APPENDIX

The reaction probability matrix for the WR mechanism that specifies the change from a particle configuration $\boldsymbol{\alpha}$ to a configuration $\boldsymbol{\beta}$ at a node for $\boldsymbol{\alpha} \neq \boldsymbol{\beta}$ is [12]

$$P(\boldsymbol{\alpha}|\boldsymbol{\beta}) = \left[p_1^+(\boldsymbol{\alpha})\,\delta_{\alpha_x+1,\beta_x} + p_1^-(\boldsymbol{\alpha})\,\delta_{\alpha_x-1,\beta_x}\right]\delta_{\alpha_y,\beta_y}\delta_{\alpha_z,\beta_z} + \left[p_2^+(\boldsymbol{\alpha})\,\delta_{\alpha_y+1,\beta_y} + p_2^-(\boldsymbol{\alpha})\,\delta_{\alpha_y-1,\beta_y}\right]\delta_{\alpha_x,\beta_x}\delta_{\alpha_z,\beta_z} + \left[p_3^+(\boldsymbol{\alpha})\,\delta_{\alpha_z+1,\beta_z} + p_3^-(\boldsymbol{\alpha})\,\delta_{\alpha_z-1,\beta_z}\right]\delta_{\alpha_x,\beta_x}\delta_{\alpha_y,\beta_y}\,, \tag{A1}$$

where the explicit expressions for $p_\tau^\pm(\boldsymbol{\alpha})$ are

$$\begin{aligned}
p_1^+(\boldsymbol{\alpha}) &= q_1^+(\boldsymbol{\alpha})(1-\delta_{\alpha_x,m}),\\
p_1^-(\boldsymbol{\alpha}) &= q_1^-(\boldsymbol{\alpha}) - q_1^+(\boldsymbol{\alpha})\delta_{\alpha_x,m}\,,\\
p_2^+(\boldsymbol{\alpha}) &= q_2^+(\boldsymbol{\alpha})(1-\delta_{\alpha_y,m}),\\
p_2^-(\boldsymbol{\alpha}) &= q_2^-(\boldsymbol{\alpha}) - q_2^+(\boldsymbol{\alpha})\delta_{\alpha_y,m}\,,\\
p_3^+(\boldsymbol{\alpha}) &= q_3^+(\boldsymbol{\alpha})(1-\delta_{\alpha_z,m}),\\
p_3^-(\boldsymbol{\alpha}) &= q_3^-(\boldsymbol{\alpha}) - q_3^+(\boldsymbol{\alpha})\delta_{\alpha_z,m}
\end{aligned} \tag{A2}$$

with

$$\begin{aligned}
q_1^+/h &= \kappa_1\alpha_x + m\kappa_{-2}\alpha_y(\alpha_y-1)/(m-1) + \kappa_{-4}\,,\\
q_1^-/h &= m\kappa_{-1}\alpha_x(\alpha_x-1)/(m-1) + (\kappa_2\alpha_y + \kappa_4\alpha_z)\alpha_x\,,\\
q_2^+/h &= \kappa_2\alpha_x\alpha_y + \kappa_{-3}\,,\\
q_2^-/h &= m\kappa_{-2}\alpha_y(\alpha_y-1)/(m-1) + \kappa_3\alpha_y\,,\\
q_3^+/h &= \kappa_5\alpha_z + \kappa_{-4}\,,\\
q_3^-/h &= \kappa_4\alpha_x\alpha_z + m\kappa_{-5}\alpha_z(\alpha_z-1)/(m-1)\,.
\end{aligned} \tag{A3}$$

The diagonal elements are $P(\boldsymbol{\alpha}|\boldsymbol{\alpha}) = 1 - \sum_{\boldsymbol{\beta}} P(\boldsymbol{\alpha}|\boldsymbol{\beta})$. The transition probabilities P_τ^+ and P_τ^- used in the text are determined from averages of the $p_\tau^\pm(\boldsymbol{\alpha})$ over the binomial distribution on $\mathcal{L}_\tau$

$$\mathcal{P}_{\rm b}(\alpha_\tau,\rho_\tau) = \frac{m!}{(m-\alpha_\tau)!\alpha_\tau!}\left(\frac{\rho_\tau}{m}\right)^{\alpha_\tau}\left(1-\frac{\rho_\tau}{m}\right)^{m-\alpha_\tau}, \tag{A4}$$

and are given by

$$P_\tau^\pm = \sum_{\boldsymbol{\alpha}} p_\tau^\pm(\boldsymbol{\alpha})\mathcal{P}_{\rm b}(\boldsymbol{\alpha},\boldsymbol{\rho})\,. \tag{A5}$$

We find

$$\begin{aligned}
P_1^+ &= \kappa_1\rho_1 + \kappa_{-2}\rho_2^2 + \kappa_{-4} - Q_1\,,\\
P_1^- &= \kappa_{-1}\rho_1^2 + \kappa_2\rho_1\rho_2 + \kappa_4\rho_1\rho_3 - Q_1\,,\\
P_2^+ &= \kappa_2\rho_1\rho_2 + \kappa_{-3} - Q_2\,,\\
P_2^- &= \kappa_{-2}\rho_2^2 + \kappa_3\rho_2 - Q_2\,,\\
P_3^+ &= \kappa_{-4} + \kappa_5\rho_3 - Q_3\,,\\
P_3^- &= \kappa_4\rho_1\rho_3 + \kappa_{-5}\rho_3^2 - Q_3\,,
\end{aligned} \tag{A6}$$

where

$$Q_\tau = \sum_{\boldsymbol{\alpha}} q_\tau^+(\boldsymbol{\alpha})\mathcal{P}_{\rm b}(\boldsymbol{\alpha},\boldsymbol{\rho})\delta_{\alpha_\tau,m}\,. \tag{A7}$$

[1] J.P. Crutchfield and B.A. Huberman, Phys. Lett. **74A**, 407 (1980); J.P. Crutchfield, J.D. Farmer, and B.A. Huberman, Phys. Rep. **92**, 47 (1982).
[2] B. Shraiman, C.E. Wayne, and P.C. Martin, Phys. Rev. Lett. **46**, 935 (1981).
[3] M.J. Feigenbaum, J. Stat. Phys. **19**, 25 (1978); **21**, 669 (1979).
[4] A. Arnéodo, in *Fluctuations and Sensitivity in Nonequilibrium Systems*, edited by W. Horsthemke and D.K. Kodepudi (Springer, Berlin, 1984).
[5] G. Mayer-Kress and H. Haken, J. Stat. Phys. **26**, 149 (1981).
[6] M.J. Feigenbaum and B. Hasslacher, Phys. Rev. Lett. **49**, 605 (1982).
[7] T. Kapitaniak, *Chaos in Systems with Noise* (World Scientific, Singapore, 1988).
[8] J. Keizer and J. Tilden, J. Phys. Chem. **93**, 2811 (1989).
[9] R.F. Fox, Phys. Rev. A **41**, 2960 (1990); **42**, 1946 (1990); R.F. Fox and J. Keizer, Phys. Rev. Lett. **64**, 249 (1990); Phys. Rev. A **43**, 1709 (1991); J.E. Keizer and R.F. Fox, *ibid.* **46**, 3572 (1992); R.F. Fox and T.C. Elston (unpublished).
[10] G. Nicolis and V. Balakrishnan, Phys. Rev. A **46**, 3569 (1992); P. Peters and G. Nicolis, Physica A **188**, 426 (1992); P. Geysermans and G. Nicolis, J. Chem. Phys. (1994).
[11] X.-G. Wu and R. Kapral, Phys. Rev. Lett. **70**, 1940 (1993); Ann. N.Y. Acad. Sci. **706**, 186 (1993); R. Kapral and X.-G. Wu, in *Chemical Waves and Patterns*, edited by R. Kapral and K. Showalter (Kluwer, Dordrecht, 1994).
[12] X.-G. Wu and R. Kapral, J. Chem. Phys. **100**, 5936 (1994).
[13] K.-D. Willamowski and O.E. Rössler, Z. Naturforsch. Teil A **35**, 317 (1980).
[14] B.D. Aguda and B.L. Clarke, J. Chem. Phys. **89**, 7428 (1988).
[15] D. Dab, A. Lawniczak, J.-P. Boon, and R. Kapral, Phys. Rev. Lett. **64**, 2462 (1990); A. Lawniczak, D. Dab, R. Kapral, and J.-P. Boon, Physica D **47**, 132 (1991).
[16] R. Kapral, A. Lawniczak, and P. Masiar, Phys. Rev. Lett. **66**, 2539 (1991); J. Chem. Phys. **96**, 2762 (1992).
[17] D. Dab, J.P. Boon, and Y.-X. Li, Phys. Rev. Lett. **66**, 2535 (1991).

[18] See, for instance, G. Nicolis and I. Prigogine, *Self-Organization in Non-Equilibrium Systems* (Wiley, New York, 1977); N. G. van Kampen, *Stochastic Processes in Physics and Chemistry* (North-Holland, Amsterdam, 1981).

[19] D. Gruner, R. Kapral, and A. Lawniczak, J. Chem. Phys. **99**, 3938 (1993); J. Weimar, D. Dab, J.P. Boon, and S. Succi, Europhys. Lett. **20**, 627 (1992).

[20] The stochastic simulations employ a small but finite value of the time scale factor h (for Figs. 1 and 6 $h = 10^{-4}$ while in the remaining simulations $h = 1.5 \times 10^{-4}$). As a result the deterministic (mean field) limit of the stochastic dynamics is the Euler discretization of the rate law given in (11). We have confirmed that, although there are small shifts in bifurcation points for this discrete system, the period-doubling cascade to chaos has the same structure in both the continuous-time and discrete mean field WR models.

[21] E.A. Celarier and R. Kapral, J. Chem. Phys. **86**, 3366 (1987).

[22] The superstable points were determined by searching for the parameter values where the character of the relaxation to a fixed point in the Poincaré section changes from monotone to oscillatory.

[23] *Lyapunov Exponents*, edited by L. Arnold and V. Wihstutz, Lecture Notes in Mathematics Vol. 1186 (Springer-Verlag, New York, 1986).

[24] H. Herzel, W. Ebeling, and Th. Schulmeister, Z. Naturforsch. Teil A **42**, 136 (1986).

[25] G. Benettin, L. Galgani, and J.-M. Strelcyn, Phys. Rev. A **14**, 2338 (1976).

[26] For a periodic orbit, the continuous-time rate law (3) has a zero Lyapunov exponent, corresponding to neutral stability along the orbit, and two negative exponents, one of which is equal to minus infinity at superstability. The Euler discretized form of this rate law (11) has three negative eigenvalues, one of which is close to zero and tends to zero as h tends to zero, and another is equal to minus infinity at superstability.

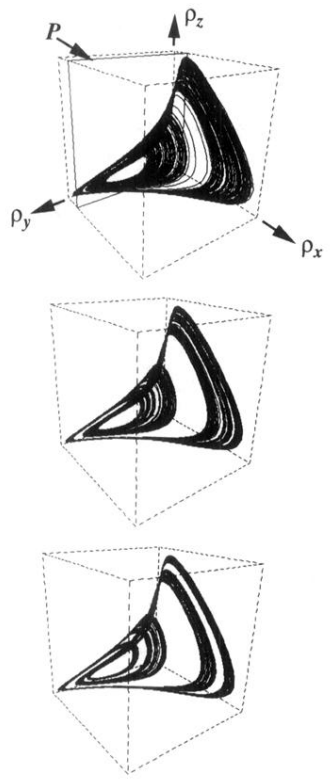

FIG. 1. Three-dimensional plot of phase-space trajectories obtained using the stochastic simulation method for $\mathcal{N} = (1024)^2$ (top) and $\mathcal{N} = (4096)^2$ (middle). The deterministic attractor is shown in the bottom panel. The bifurcation parameter was chosen so that the system is in the chaotic regime, i.e., $\kappa_2 = 1.571$, and the trajectories were obtained by following the motion of phase point $\rho_\tau(t) = n_\tau(t)/\mathcal{N}$ in the three-dimentional concentration phase space. The dashed box containing the attractor has its origin at $(0.070\,64, 0.002\,76, 0.111\,90)$ and corners along the ρ_x, ρ_y, and ρ_z axes at 1.801 29, 1.759 82, and 4.287 91, respectively. The Poincaré section, defined in (17), is shown in the top panel and labeled by $\mathcal{P}$.

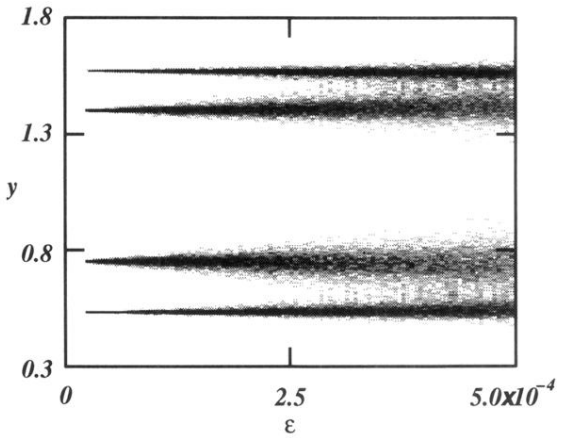

FIG. 7. Noise bifurcation diagram for $\kappa_2 = 1.537$ (superstable period-4 orbit). The ordinate y is the ρ_y value on $\mathcal{P}$.